

**Raymond Mejia and James B. Wade**

*Am J Physiol Renal Physiol* 282:553-557, 2002. First published Nov 13, 2001;  
doi:10.1152/ajprenal.00340.2000

**You might find this additional information useful...**

---

This article has been cited by 4 other HighWire hosted articles:

**A model of glucose transport and conversion to lactate in the renal medullary microcirculation**

W. Zhang and A. Edwards

*Am J Physiol Renal Physiol*, January 1, 2006; 290 (1): F87-F102.

[Abstract] [Full Text] [PDF]

**Chloride Transport in the Kidney: Lessons from Human Disease and Knockout Mice**

T. J. Jentsch

*J. Am. Soc. Nephrol.*, June 1, 2005; 16 (6): 1549-1561.

[Abstract] [Full Text] [PDF]

**Determinants of basal nitric oxide concentration in the renal medullary microcirculation**

W. Zhang, T. Pibulsonggram and A. Edwards

*Am J Physiol Renal Physiol*, December 1, 2004; 287 (6): F1189-F1203.

[Abstract] [Full Text] [PDF]

**Three-dimensional functional reconstruction of inner medullary thin limbs of Henle's loop**

T. L. Pannabecker, D. E. Abbott and W. H. Dantzer

*Am J Physiol Renal Physiol*, January 1, 2004; 286 (1): F38-F45.

[Abstract] [Full Text] [PDF]

Updated information and services including high-resolution figures, can be found at:

<http://ajprenal.physiology.org/cgi/content/full/282/3/F553>

Additional material and information about *AJP - Renal Physiology* can be found at:

<http://www.the-aps.org/publications/ajprenal>

---

This information is current as of July 5, 2009 .

# Immunomorphometric study of rat renal inner medulla

RAYMOND MEJIA<sup>1</sup> AND JAMES B. WADE<sup>2</sup>

<sup>1</sup>Mathematical Research Branch, National Institutes of Health, Bethesda 20892-2690; and

<sup>2</sup>Department of Physiology, University of Maryland School of Medicine, Baltimore, Maryland 21201

Received 14 December 2000; accepted in final form 31 October 2001

**Mejia, Raymond, and James B. Wade.** Immunomorphometric study of rat renal inner medulla. *Am J Physiol Renal Physiol* 282: F553–F557, 2002. First published November 13, 2001; 10.1152/ajprenal.00340.2000.—We utilized immunofluorescent immunolabeling of renal tissue sections to identify and count tubules at specified depths of the rat renal inner medulla. We used primary antibodies to aquaporin-1 (AQP1; labeling thin descending limbs), aquaporin-2 (AQP2; labeling inner medullary collecting ducts), the rat kidney-specific chloride channel (ClC-K1; labeling thin ascending limbs), and von Willebrand factor (labeling descending vasa recta). Secondary antibodies conjugated to different fluorophores were used, giving up to a three-color display. Labeled structures were then identified and counted. At each level sampled in the inner medulla, many more thin limbs were labeled by ClC-K1 than AQP1. In addition, thin limbs were found to label with antibodies to ClC-K1 on both sides of their hairpin turns. We conclude that the descending thin limbs shift from expressing AQP1 to expressing ClC-K1 some distance before the point where they turn and begin to ascend. Mathematical models can use our quantitative data to explore implications for the urine-concentrating mechanism.

loop of Henle; urine-concentrating mechanism; inner medulla; aquaporin; chloride channel; urea channel

WATER ABSORPTION FROM THE descending limbs of Henle's loop is of primary importance for the concentrating ability of the mammalian kidney, because ~90% of filtered water is reabsorbed before it reaches the cortical collecting duct. Reports in the literature describe water- and solute-permeable descending limbs in hamsters (8, 19), rats (1, 3, 9), chinchillas (1, 2, 6), and rabbits (10, 13, 21). The descending limb of Henle's loop has been found in all species to be water permeable and moderately permeable to NaCl and urea. The adjacent ascending thin limb (ATL) of Henle's loop is characterized by extremely low water permeability and very high chloride permeability (7).

Chou et al. (1) showed that the osmotic water permeability of the descending limb in chinchillas is not uniformly high along its length. Instead, the distal 20% of the long-loop descending thin limb (DTL) was shown to have a relatively low water permeability (50  $\mu\text{m/s}$ ). Chou et al. (2) also showed the NaCl and urea permeabilities to be nonuniform in the chinchilla descending

limb, attaining a maximum in the innermost segment of 98.4 and 47.6  $\mu\text{m/s}$ , respectively.

Osvaldo and Latta (24) used electron microscopy to examine different levels of the inner medulla to characterize the structure of thin limbs of the rat kidney. Kriz and colleagues (16, 17) and Dieterich et al. (5) expanded these observations in their characterizations of thin limbs in mouse and other species. Osvaldo and Latta observed that, in a cross section from the upper layer of the inner medulla, there are "complex" (identified as DTL) and "simple" (identified as ATL) thin limbs and that the structure of the complex type becomes more simplified as they descend. They further suggested that for the longest loops a transition from complex to simple epithelium might occur at variable levels within the descending segment. This would explain the predominance of simple thin limbs found toward the papillary tip.

Dieterich et al. (5) described four types of epithelia. Type 1 epithelia, characteristic of short loops, were the smallest in diameter and had the thinnest cells. Types 2, 3, and 4 were found in the long loops. Type 2 epithelia occur in the inner stripe of the outer medulla. Type 3 epithelia, distal to type 2, were smaller than type 2, with a smaller diameter than type 2 but one greater than that of type 1. Type 3 cells appeared to be less specialized than those of type 2. The ascending thin limbs form type 4, with the epithelium appearing to be simple relative to the other types. Furthermore, the transition from type 3 to type 4 was found to occur some distance before the bend of the loop of Henle (5). Early morphological studies in rats, mice, and rabbits (15) lacked the markers needed to evaluate the distribution of transporters in the different regions described.

Recently, Pannabecker et al. (25) have shown that, for multiple species, many inner medullary thin limbs exhibit structural characteristics of DTL immediately adjacent to segments with structural characteristics of ATL at sites above the bend. They have shown that AQP1 is expressed in the DTL-type but not in ATL-type regions of these mixed-type thin limbs, whereas the chloride channel ClC-K1 is expressed in ATL-type but not in DTL-type regions of mixed-type thin limbs.

AQP1 is a constitutively active water channel found in DTLs and in descending vasa recta (DVR) in rat

Address for reprint requests and other correspondence: R. Mejia, BSA Bldg., Suite 350, National Institutes of Health, Bethesda, MD 20892-2690 (E-mail: ray@helix.nih.gov).

The costs of publication of this article were defrayed in part by the payment of page charges. The article must therefore be hereby marked "advertisement" in accordance with 18 U.S.C. Section 1734 solely to indicate this fact.

kidney, but not found in ATLs (18, 23). CIC-K1 is found in ATL cells (29, 30) and in ATL-type DTL segments (2, 5). On the other hand, AQP2 is a water channel found in collecting duct principal cells and in inner medullary collecting duct cells (22).

Here, we used immunofluorescent immunolabeling of tissue sections to identify and count AQP1, AQP2, and CIC-K1-positive tubules in rat inner medulla. The data obtained give an estimate of the fraction of descending limbs that are water permeable and the fraction that are solute permeable at a given distance from the papillary tip. The data also serve to estimate the number and diameter of tubules that extend to various depths of the inner medulla, which are important for mathematical models of the urine-concentrating mechanism (26, 20) that use the number and dimensions of loops of Henle and their transport properties as parameters.

## METHODS

**Experimental animals.** In view of evidence that CIC-K1 expression may be regulated by vasopressin (30), all tissue for immunocytochemistry was taken from animals exposed to high levels of vasopressin. Three male Brattleboro rats (210–260 g, Harlan Sprague Dawley, Indianapolis, IN) were implanted with osmotic minipumps (Alzet model 2001, Alza, Palo Alto, CA) to administer 20 ng/h 1-desamino-8-D-arginine vasopressin, the V<sub>2</sub> receptor-selective agonist of vasopressin. In addition, tissue from three male Sprague-Dawley rats (200–225 g) was also examined. These animals were maintained on a water-restricted diet for 5 days as previously described by Kim et al. (11).

**Antibodies.** To perform immunolocalization studies, we used peptide-directed polyclonal antibodies to 1) AQP1, raised in rabbits (L266) and chickens (LC18), to the same peptide (28); 2) CIC-K (COOH-terminal peptide of CIC-K2, KKAI<sup>ST</sup>LINPARK), kindly provided by Klaus Steinmeyer, that recognizes both CIC-K1 and CIC-K2 (30) or CIC-K antibody (AB5392; Chemicon, Temecula, CA); 3) von Willebrand factor (vWF; Cedarlane Labs, Ontario, PQ); and 4) AQP2 raised in guinea pigs [GP7; COOH-terminal peptide of AQP2 to the same peptide previously used to produce antibodies in rabbits (22)].

**Fixation of tissue and immunocytochemistry.** Kidneys of ketamine-pentobarbital-anesthetized animals were fixed for immunolocalization by retrograde perfusion through the abdominal aorta, and antibodies were immunolocalized on frozen sections as previously described by Wade et al. (31). Sections, usually 12  $\mu$ m thick and beginning at the papillary tip, were counted to obtain an estimate of the distance of each section from the papilla. The sections were incubated overnight at 4°C with primary antibodies diluted to 10  $\mu$ g/ml. Secondary antibodies were species-specific donkey anti-chicken, donkey anti-rabbit, and donkey anti-guinea pig antibodies (Jackson ImmunoResearch Labs, West Grove, PA) coupled to Alexa 488, Alexa 568 (Molecular Probes, Eugene, OR), and Cy5, respectively.

**Data analysis.** Immunofluorescent-labeled tissue cross sections were used to identify and count the number of tubules labeled by each fluorophore. The number of AQP1-labeled plus the number of CIC-K1-labeled tubules minus the number of AQP1- and vWF-labeled vasa recta serves to estimate the number of descending and ascending limbs of the loop of Henle in a cross section at each distance from the papillary tip. Because one-half of the limbs of Henle's loop at each

medullary depth are descending and one-half ascending, we approximated the number of descending limbs in each cross section as one-half of the total number of limbs present in the cross section.

## RESULTS

**Immunofluorescent localization in rat inner medulla.** We used triple immunofluorescent immunolabeling of cross sections from the tip and from the base of the inner medulla. Figure 1 shows immunofluorescent labeling of a section of inner medulla from a 1-desamino-8-D-arginine vasopressin-infused Brattleboro rat. Secondary antibodies are conjugated to different fluorophores, giving a three color display. The 0.25-mm<sup>2</sup> section is  $\sim$ 840  $\mu$ m from the papillary tip. CIC-K1 is labeled red and is localized in ATL-type limbs of Henle's loop; AQP1-sensitive structures are labeled green, and AQP2-sensitive collecting duct cells are labeled blue.

We counted individual tubule types, namely, DTL, ATL, and collecting ducts, at distinct depths in the inner medulla using AQP1 to label DTL, AQP2 to label collecting duct, CIC-K1 to label ATL, and vWF to label DVR. The latter is used to distinguish DVR from DTL, both of which express AQP1. This is shown in Fig. 2, which is a section  $\sim$ 828  $\mu$ m from the tip. AQP1 appears in green; CIC-K1 in red, and vWF in blue. DVR, labeled blue, are smaller in outer diameter and cell height than DTL, labeled green.

Nearly all thin limb structures were either labeled by CIC-K1 antibody or AQP1. Occasionally, thin limbs were encountered that displayed labeling by both antibodies. These observations are most easily

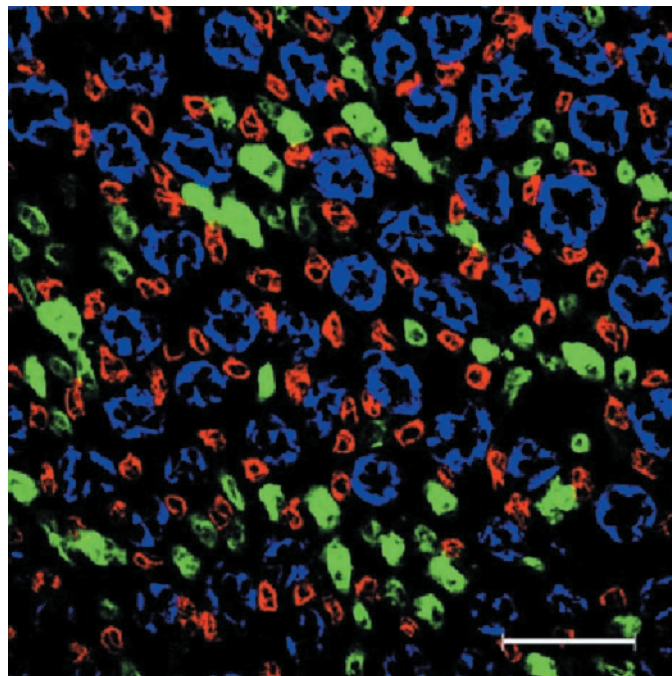


Fig. 1. Section ( $\sim$ 0.25 mm<sup>2</sup>) taken  $\sim$ 840  $\mu$ m from the tip of the papilla. Rat-kidney-specific chloride channel (CIC-K1) is labeled in red, aquaporin-1 (AQP1) in green, and AQP2 in blue. Bar, 100  $\mu$ m.

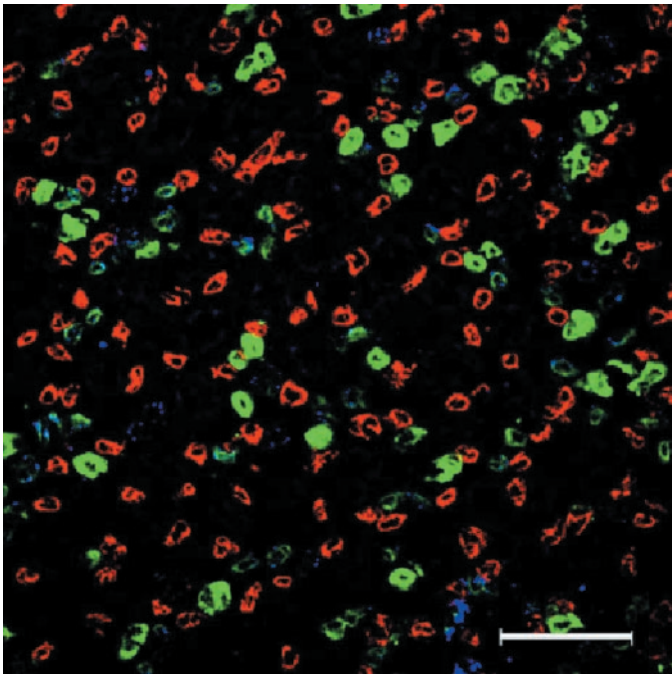


Fig. 2. Section taken  $\sim 828 \mu\text{m}$  from the papillary tip. AQP1 is labeled in green; ClC-K1 in red, and von Willebrand factor in blue. Bar,  $100 \mu\text{m}$ .

explained as representing transitional regions between regions with a DTL-type epithelium and an adjacent ATL-type epithelium. Such transitional regions were most frequent near the tip of the papilla. An example of the labeling seen in this region is shown in Fig. 3. There are limbs that label strongly with antibody to ClC-K1 (ATL) and some that label weakly (Fig. 3A). Some of the weakly labeled limbs (arrows) are also partially labeled with AQP1 (Fig. 3B). The finding that regions with transitional labeling can be identified suggests that DTLs expressing AQP1 transition directly into regions expressing ClC-K1 (albeit at a low level) without an intervening region that lacks either transporter. Although it may

be that some DTLs have short regions that lack detectable labeling, this finding indicates that our counts of labeled limbs are likely to correspond to the incidence of thin limbs.

The number of loops of Henle at a given distance from the papillary tip to the junction of the inner and outer medulla is shown in Table 1. The number of ATL-type tubules labeled by chloride channel antibody at each depth is shown in the second column of the table, followed by the AQP1-positive DTL. Where the vWF antibody has been used, the number of DVR has been subtracted from the total of AQP1-positive tubules; where vWF antibody has not been used, the distinction has been made based on morphology. The incidence of loops of Henle was then estimated as one-half of the total number of limbs labeled in the section. The percentage of DTLs that express AQP1 is shown in Table 1 (column 5). The standard deviation is shown where several  $0.25\text{-mm}^2$  sections have been averaged at a given level in the medulla.

Table 1 shows that the incidence of ClC-K1-labeled limbs greatly exceeds the number labeled by AQP1 for each level of the inner medulla. The incidence of ClC-K1 labeling that we estimate to occur in DTLs ranges from  $\sim 60\%$  at the base of the inner medulla to  $30\text{--}40\%$  near the tip of the papilla. One explanation for this labeling pattern is that DTLs begin to express ClC-K1 and assume an ATL character before turning and becoming ATLs. To determine whether this is true, we examined longitudinal sections through the inner medulla for sections that show sites of turning thin limbs. As shown in Fig. 4, turning thin limbs could be identified in such sections, and in each case they displayed ClC-K1 labeling on both sides of the turn (arrows, Fig. 4). Note also that Table 1 shows that the fraction of AQP1-positive descending limbs decrease with medullary depth. This is consistent with our evidence that AQP1-expressing DTLs change into ClC-K1-expressing regions before they turn. The last two columns of Table 1 show an estimate of the number of ClC-K1-labeled descending limbs of the loop of Henle

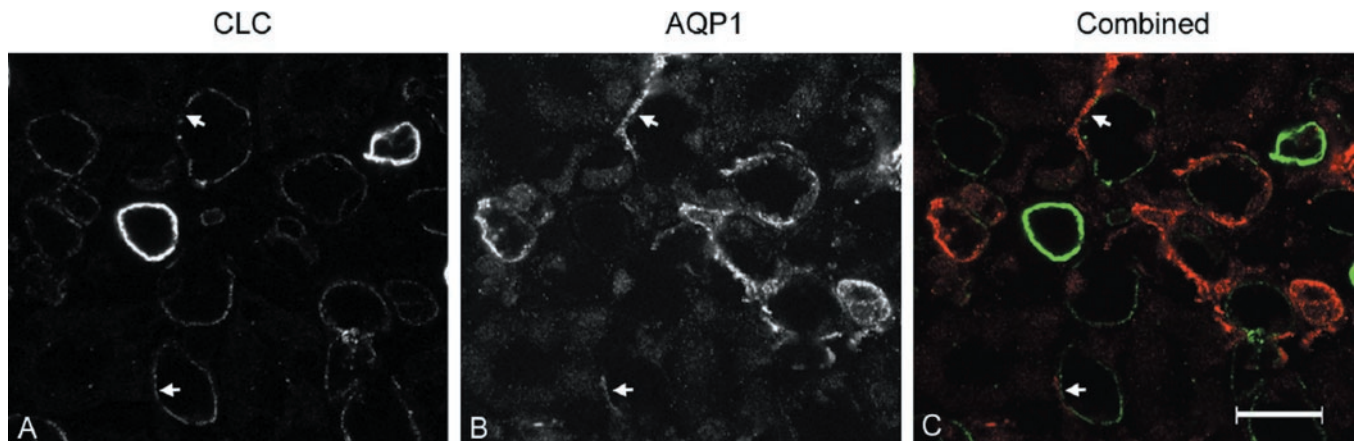


Fig. 3. Immunolabeling in transitional regions. This section is  $\sim 50 \mu\text{m}$  from the tip of the papilla. A: limbs with strong and weak ClC-K1 labeling. B: AQP1 labeling showing that some of the limbs labeled weakly by ClC-K1 are also labeled by AQP1 (arrows). C: combined ClC-K1 (green) and AQP1 (red) images. Bar,  $25 \mu\text{m}$ .

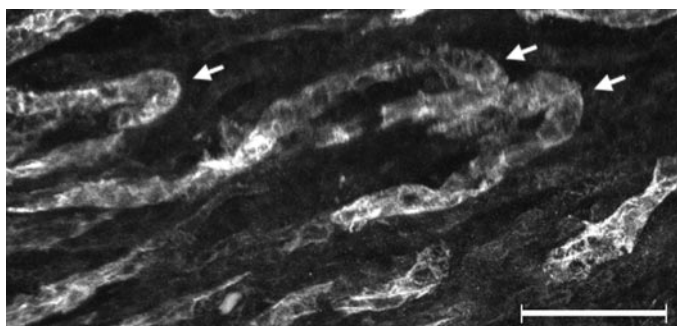


Fig. 4. Immunolabeling by CIC-K1 antibody in turning thin limbs. This longitudinal section through the inner medulla shows that turning thin limbs (arrows) are labeled by CIC-K1 antibody on both sides of the turn. The image is a z-axis projection of 45 1- $\mu$ m optical sections. Labeling for AQP1 did not detect any labeling in the tubule loops by CIC-K1 (not shown). Bar, 100  $\mu$ m.

and the number of inner medullary collecting ducts. Note that the number of collecting ducts tends to decrease as medullary depth increases.

Luminal diameter changes along the DTL and ATL have been measured (17, 12). We have estimated tubule diameters by measuring tubules cut in a circular or elliptical pattern. In the latter case, we have computed the diameter of the circle obtained from the ellipse by a continuous transformation. In this manner, we estimated luminal diameters of 12–14  $\mu$ m for both DTL- and ATL-type tubules near the base of the inner medulla. Near the papillary tip, we computed, for ATL-type tubules, inner diameters of 11–12  $\mu$ m and outer diameters of 17–19  $\mu$ m. Outer diameters of transitional segments, reported to have taller cells (17), are estimated to be 20–26  $\mu$ m.

**DISCUSSION**

Data summarized in Table 1 show that CIC-positive limbs of Henle’s loop exceed AQP1-positive limbs of Henle’s loop at all medullary depths and cross sections studied. On average, one expects that one-half of the limbs of Henle’s loop will be descending, and Table 1 shows 62–11% of descending limbs to be AQP1 positive for Brattleboro rats, whereas the fraction that are

AQP1 positive decrease and the fraction that are CIC positive increase toward the papillary tip. Panna-becker et al. (25) reported that ~55% of thin limbs isolated from distinctly above the bend of the loop were of the mixed type, meaning that they expressed both AQP1 and CIC-K1 somewhere along their length. Our findings suggest that the incidence of regions expressing AQP1 decreases substantially near the papillary tip, and we estimate that ~70–90% of DTLs are CIC positive near the tip of the papilla.

Data for 0.25-mm<sup>2</sup> sections show a maximum of 110 limbs of Henle’s loop turning/section within 900  $\mu$ m of the tip and 30 limbs turning/0.25-mm<sup>2</sup> section nearest the tip. This is comparable to the 400 and 90/mm<sup>2</sup>, respectively, reported by Knepper et al. (12) (Fig. 4). Table 1 also shows the number of inner medullary collecting ducts and ATLs to approach asymptotically near the papillary tip, which was shown previously (20), and data for Sprague-Dawley rats that were water-restricted are shown to be consistent with that for Brattleboro rats.

*Implications for mathematical models.* The mechanism utilized by the mammalian kidney to generate a concentration gradient in the inner medulla is still unclear after decades of study (see review in Ref. 4). One possible mechanism is water absorption from thin descending limbs in conjunction with a preferential solute reabsorption from thin ascending limbs and countercurrent multiplication (14, 26).

In vitro perfusion studies of thin descending limbs in hamsters (8), rats (1), and chinchillas (1, 2) have demonstrated a water-permeable descending limb. Low-to-moderate solute permeabilities have been measured for several species in DTL, e.g., sodium permeability in hamsters (8) and NaCl permeability in chinchillas (1, 2). In addition, little or no Na<sup>+</sup>,K<sup>+</sup>-ATPase activity has been recorded in thin descending limbs in the inner medulla, e.g., in rats (27). The measurements from perfusion studies and the data from immunolocalization suggest that mathematical models of the urine-concentrating mechanism might investigate a distribution of water- and solute-transporting segments of DTL on the basis of the distribution of AQP1 and CIC

Table 1. Labeled tubules and estimates of DTL, ATL, and IMCD

Distance to Tip, $\mu$ m	CIC-Labeled, no./0.25 mm <sup>2</sup>	AQP1-Labeled DTL*	Estimated Incidence of Loops†	%AQP1-Labeled DTL	CIC-Labeled DTL, no./0.25 mm <sup>2</sup>	IMCD, no./0.25 mm <sup>2</sup>
<i>Sprague-Dawley rats</i>						
0 < 200 (7)	78 ± 20	14 ± 2	46 ± 10	30	32 ± 10	37 ± 2(3)
200 < 400 (6)	104 ± 15	33 ± 17	69 ± 15	49	35 ± 7	36 ± 21
Base of IM (2)	190 ± 33	72 ± 21	131 ± 27	55	59 ± 6	118 ± 6
<i>Brattleboro rats</i>						
0 < 200 (3)	84 ± 27	5 ± 4	45 ± 13	11	39 ± 15	29 ± 5
200 < 400 (7)	75 ± 23	14 ± 4	44 ± 12	32	30 ± 11	37 ± 8
400 < 900 (12)	112 ± 22	31 ± 14	71 ± 18	44	40 ± 6	56 ± 4(6)
Base of IM (3)	216 ± 21	97 ± 10	156 ± 15	62	60 ± 6	70 ± 10(2)

Values are means ± SD with average no. of sections at that depth in parentheses. DTL, descending thin limbs; ATL, ascending thin limbs; IMCD, inner medullary collecting ducts; IM, inner medulla; CIC, chloride channel; AQP1, aquaporin-1. \*No. (no./0.25 mm<sup>2</sup>) of AQP1-labeled DTL = structures labeled by AQP1 – descending vasa recta (DVR). †Estimated incidence (no./0.25 mm<sup>2</sup>) of loops = (AQP1 + CIC)/2.

channels observed. Our observations, as well as those of others (25), show transitions from AQP1-positive to CIC-positive segments with no significant colocalization of solute and water channels. Hence, mathematical models might test the effect of water-permeable segments of DTL juxtaposed and in series with solute-permeable segments of DTL on solute concentration gradients in the inner medulla and on the kidney's ability to concentrate urine.

**Conclusion.** We conclude that, at distinct axial distances within the inner medulla, a variable fraction of DTL cells express AQP1 compared with those expressing CIC-K1. Our observations suggest that a smaller fraction of the DTL at each depth are water permeable than are carrying out solute transport. The finding that the proportion labeled by AQP1 falls axially suggests that water reabsorption from DTL may diminish near the tip of the inner medulla. Mathematical models of the urine-concentrating mechanism can use this data to explore possible implications for the urine-concentrating mechanism.

The authors gratefully acknowledge the encouragement and very helpful advice of Dr. Mark Knepper of the National Institutes of Health. We also appreciate the expert technical assistance of Jie Liu. Images were processed with IDL version 5.2, Research Systems, Inc., on the Helix System of the Center for Information Technology at the National Institutes of Health.

This study was supported by National Institutes of Health Grant DK-32839 (J. B. Wade). Brattleboro rats with 1-desamino-8-D-arginine vasopressin minipumps were provided by Dr. James Terris of the Uniformed Services University. Polyclonal antibody was kindly provided by Dr. Klaus Steinmeyer of the University of Hamburg.

## REFERENCES

1. **Chou C-L and Knepper MA.** In vitro perfusion of chinchilla thin limb segments: segmentation of osmotic water permeability. *Am J Physiol Renal Fluid Electrolyte Physiol* 263: F471–F476, 1992.
2. **Chou C-L and Knepper MA.** In vitro perfusion of chinchilla thin limb segments: urea and NaCl permeabilities. *Am J Physiol Renal Fluid Electrolyte Physiol* 264: F337–F343, 1993.
3. **Chou C-L, Knepper MA, Hoek AN, Brown D, Yang B, Ma T, and Verkman AS.** Reduced water permeability and altered ultrastructure in thin descending limb of Henle in aquaporin-1 null mice. *J Clin Invest* 103: 491–496, 1999.
4. **Chou C-L, Knepper MA, and Layton HE.** Urinary concentrating mechanism: the role of the inner medulla. *Semin Nephrol* 13: 168–181, 1993.
5. **Dietrich HJ, Barrett JM, Kriz W, and Bulhoff JP.** The ultrastructure of the thin loop limbs of the mouse kidney. *Anat Embryol* 147: 1–18, 1975.
6. **Flessner MF, Mejia R, and Knepper MA.** Ammonium and bicarbonate transport in isolated perfused rodent long-loop thin descending limbs. *Am J Physiol Renal Fluid Electrolyte Physiol* 264: F388–F396, 1993.
7. **Imai M and Kokko JP.** Sodium chloride, urea, and water transport in the thin ascending limb of Henle. Generation of osmotic gradients by passive diffusion of solutes. *J Clin Invest* 53: 393–402, 1974.
8. **Imai M, Taniguchi J, and Yoshitomi K.** Transition of permeability properties along the descending limb of long-loop nephron. *Am J Physiol Renal Fluid Electrolyte Physiol* 254: F323–F328, 1988.
9. **Jamison RL, Buerkert J, and Lacy F.** A micropuncture study of Henle's thin loop in Brattleboro rats. *Am J Physiol* 224: 180–185, 1973.
10. **Johnston PA, Battilana CA, Lacy FB, and Jamison RL.** Evidence for a concentration gradient favoring outward movement of sodium from the thin loop of Henle. *J Clin Invest* 59: 234–240, 1977.
11. **Kim GH, Ecelbarger C, Mitchell C, Packer RK, Wade JB, and Knepper MA.** Vasopressin increases Na-K-2Cl cotransporter expression in thick ascending limb of Henle's loop. *Am J Physiol Renal Physiol* 276: F96–F103, 1999.
12. **Knepper MA, Danielson RA, Saidel GM, and Post RS.** Quantitative analysis of renal medullary anatomy in rats and rabbits. *Kidney Int* 12: 313–323, 1977.
13. **Kokko JP.** Sodium chloride and water transport in the descending limb of Henle. *J Clin Invest* 49: 1838–1846, 1970.
14. **Kokko JP and Rector FC Jr.** Countercurrent multiplication system without active transport in inner medulla. *Kidney Int* 2: 214–223, 1972.
15. **Kriz W.** Differences in the cytological organization of the epithelia of loops of Henle. *Curr Probl Clin Biochem* 6: 320–327, 1976.
16. **Kriz W and Koepsell H.** The structural organization of the mouse kidney. *Z Anat Entwicklungsgesch* 144: 137–163, 1974.
17. **Koepsell H, Kriz W, and Schnermann J.** Pattern of luminal diameter changes along the descending and ascending thin limbs of the loop of Henle in the inner medullary zone of the rat kidney. *Z Anat Entwicklungsgesch* 138: 321–328, 1972.
18. **Maeda Y, Smith BL, Agre P, and Knepper MA.** Quantification of aquaporin-CHIP water channel protein in microdissected renal tubules by fluorescence-based ELISA. *J Clin Invest* 95: 422–428, 1995.
19. **Marsh DJ.** Solute and water flows in the thin limbs of Henle's loop in the hamster kidney. *Am J Physiol* 218: 824–831, 1970.
20. **Mejia R, Sands JM, Stephenson JL, and Knepper MA.** Renal actions of atrial natriuretic factor: a mathematical modeling study. *Am J Physiol Renal Fluid Electrolyte Physiol* 257: F1146–F1157, 1989.
21. **Miwa T and Imai M.** Flow-dependent water permeability of the rabbit descending limb of Henle's loop. *Am J Physiol Renal Fluid Electrolyte Physiol* 245: F743–F754, 1983.
22. **Nielsen S, DiGiovanni SR, Christensen EI, Knepper MA, and Harris HW.** Cellular and subcellular immunolocalization of vasopressin-regulated water channel in rat kidney. *Proc Natl Acad Sci USA* 90: 11663–11667, 1993.
23. **Nielsen S, Pallone T, Smith BL, Christensen EI, Agre P, and Maunsbach AB.** Aquaporin-1 water channels in short and long loop descending thin limbs and in descending vasa recta in rat kidney. *Am J Physiol Renal Fluid Electrolyte Physiol* 268: F1023–F1037, 1995.
24. **Osvaldo L and Latta H.** The thin limbs of the loop of Henle. *J Ultrastructure Res* 15: 144–168, 1966.
25. **Pannabecker TL, Dahlmann A, Brokl OH, and Dantzer WH.** Mixed descending- and ascending-type thin limbs of Henle's loop in mammalian renal inner medulla. *Am J Physiol Renal Physiol* 278: F202–F208, 2000.
26. **Stephenson JL.** Concentration of urine in a central core model of the renal counterflow system. *Kidney Int* 2: 85–94, 1972.
27. **Terada Y and Knepper MA.** Na<sup>+</sup>-K<sup>+</sup>-ATPase activities in renal tubule segments of rat inner medulla. *Am J Physiol Renal Fluid Electrolyte Physiol* 256: F218–F223, 1989.
28. **Terris J, Ecelbarger CA, Nielsen S, and Knepper MA.** Long-term regulation of four renal aquaporins in rats. *Am J Physiol Renal Fluid Electrolyte Physiol* 271: F414–F422, 1996.
29. **Uchida S, Sasaki S, Nitta K, Uchida K, Horita S, Nihei H, and Marumo F.** Localization and functional characterization of rat kidney-specific chloride channel, CIC-K1. *J Clin Invest* 95: 104–113, 1995.
30. **Vandewalle A, Cluzeaud F, Bens M, Kieferle S, Steinmeyer K, and Jentsch TJ.** Localization and induction by dehydration of CIC-K1 chloride channels in the rat kidney. *Am J Physiol Renal Physiol* 272: F678–F688, 1997.
31. **Wade JB, Lee AJ, Liu J, Ecelbarger CA, Mitchell C, Bradford AD, Terris J, Kim GH, and Knepper MA.** UT-A2: a 55-kDa urea transporter in thin descending limb whose abundance is regulated by vasopressin. *Am J Physiol Renal Physiol* 278: F52–F62, 2000.